ROBUST CONTROL OF SYSTEMS WITH HYPERBOLIC PARTIAL DIFFERENTIAL EQUATIONS

PIERRE APKARIAN[1] AND DOMINIKUS NOLL[2]

ABSTRACT. We discuss strategies to bring H_∞-control techniques into play when the system dynamics are modeled by hyperbolic partial differential equations, or more generally, by systems with non-sectorial pole pattern.

KEY WORDS. Multidisk H_∞-control · non-smooth optimization · frequency domain technique · hyperbolic PDE · non-sectorial systems · boundary feedback · Euler-Bernoulli beam · Timoshenko beam · Kelvin-Voigt damping

MSC 2020. 93B36 · 93B52 · 93C20 · 90C56 · 90C90

1. INTRODUCTION

Highly oscillatory systems arise commonly in aerospace control and other high technology fields, and their modeling potentially calls for hyperbolic partial differential equations. For practitioners this rises the question whether such infinite-dimensional oscillatory models are convenient for control, or whether they are better advised to continue to rely on more traditional finite-dimensional approximations based e.g. on identification routines, or reduced-order models.

The answer may depend on whether H_∞-control strategies, fairly well-established for finite-dimensional systems, may still be brought to work for such infinite-dimensional systems. Here we understand H_∞-control as of embedding the system G in a generalized plant P and solving a multi-objective optimization problem of the form

$$\begin{array}{ll} \text{minimize} & \max\limits_{i\in S} \|T_{w_i z_i}(P,K)\|_\infty \\ \text{subject to} & \max\limits_{i\in H} \|T_{w_i z_i}(P,K)\|_\infty \le 1, \\ & K \in \mathscr{K} \text{ stabilizes } G \end{array} \tag{1}$$

with $w_i \to z_i$ designer-chosen robustness or performance channels built into P, divided into soft $i \in S$ and hard $i \in H$ constraints, and where $\mathscr{K}$ is a designer-specified class of structured, typically conveniently implemented finite-dimensional controllers; cf. [1]. The purpose of this note is to demonstrate that while the infinite-dimensional line encounters no principled difficulties for parabolic equations, hyperbolic systems may still be handled reliably under suitable precautions.

The main obstruction to frequency analysis and controller synthesis of hyperbolic systems is that they exhibit an infinity of poles arranged on vertical strips in the complex plane. When unstable, this prevents use of standard tools like the Nyquist test or the use of the system spectral abscissa [2], often used to find stabilizing controllers. But even when this string of poles is on the stable half plane, proximity to the imaginary axis still leads to strange behavior causing difficulties in synthesis. Finite-dimensional approximations of such systems G inevitably miss high frequency resonant poles with non-negligible

[1]ONERA, Department of System Dynamics, Toulouse, France.
[2]Institut de Mathématiques, Université de Toulouse, France.

magnitude, which is why practitioners may have a point in considering these G unrealistic. If the use of hyperbolic equations for control is to pass muster, it has to demonstrate its ability to provide practical controllers which are robust with regard to such highly oscillatory modes.

When systems of PDEs are considered, the distinction between hyperbolic and parabolic equations is no longer helpful, and a better way to describe the situation is to distinguish between sectorial and non-sectorial operators, or semi-groups. When the operator is not sectorial, then the mentioned difficulties caused by poles with arbitrary high frequencies close to the imaginary axis are felt, while in a sectorial system exceedingly high frequency dynamics die out quickly. Here we present a general algorithmic approach capable to deal with such non-sectorial systems, and then demonstrate its ability by controlling a Timoshenko and an Euler-Bernoulli beam.

The structure of the paper is as follows. We present our algorithm in Section 2 and comment on the individual steps in the subsections, highlighting potential difficulties caused by non-sectorial pole pattern. In the sequel, we use two studies, boundary control of a cantilever Timoshenko beam, and piezo-electric control of an Euler-Bernoulli beam, to demonstrate the mentioned difficulties with these hyperbolic systems. Section 3 briefly presents the cantilever Timoshenko beam model, where we prepare three settings, undamped, viscous damping, and Kelvin-Voigt damping. This leads to 2×2 MIMO-control problems. Section 4 recalls the Euler-Bernoulli beam model, controlled by a collocated piezoelectric sensor-actuator pair, again with the options undamped, viscous, and Kelvin-Voigt damping. H_∞-synthesis for the Timoshenko beam is discussed in Section 5, and for the Euler-Bernoulli beam in Section 6, showing how the mentioned difficulties can be overcome. Conclusions are drawn in Section 7.

2. Algorithmic scheme

In [3, 4, 5, 6, 7], we have developed a general frequency-based approach to H_∞- or H_2-control based on (1), which can be presented as follows:

Algorithm: H_∞-control of infinite-dimensional systems G

1: **Steady-state.** Compute steady state of non-linear system $G_{\rm nl}$, shift it to origin, and obtain linearization G.
2: **Transfer function.** Compute transfer function $G(s)$.
3: **Controller structure.** Choose practical controller structure $\mathscr{K}$ and find initial controller $K_0 \in \mathscr{K}$ stabilizing the loop (G, K_0).
4: **Plant.** Embed G into plant P with closed-loop performance and robustness specifications. Possibly give special attention to strong non-linearity in $G_{\rm nl}$.
5: **Optimize.** Use non-smooth optimization to solve the multidisk H_∞-optimization program (1), maintaining stability of the loop (G, K) at iterates $K \in \mathscr{K}$. Obtain optimal structured H_∞-controller $K^* \in \mathscr{K}$.
6: **Simulation.** Simulate linear closed loop (G, K^*) to verify whether robustness and performances are satisfactory. If not, modify plant P and specifications, and go back to step 5.
7: **Non-linear simulation.** Simulate non-linear closed loop $(G_{\rm nl}, K^*)$ to verify whether design is satisfactory.

We would naturally hope that this scheme remains to a large degree general, with only minimal amendments in a given particular case. This is indeed the case for sectorial systems as for instance seen with parabolic PDEs. The scheme become more case-dependent

when the pole pattern is not sectorial, and in particular, when hyperbolic partial differential equations contribute to the dynamics.

In the remainder of this section, we go through the steps of the algorithm, discuss their implementation, and comment on the challenges caused by non-sectorial dynamics.

2.1. **Comments on Step 2.** We start by noticing that step 2 is not always available analytically. Rather shall we have to compute $G(s)$ using the numerical solution of an elliptic boundary value problem for a sufficiently dense set $s_\nu = j\omega_\nu$ of frequencies. More formally, if a boundary control system is given under the form

$$G : \begin{cases} \dot{x} = Ax \\ Px = u \\ y = Cx \end{cases} \tag{2}$$

with suitable operators A, P, C, see [9, Sect. 3.3], then computation of a single $G(s)$ is obtained by applying the Laplace transform to (2) and solving the elliptic boundary value problem

$$G(s) : \begin{cases} sx(s) = Ax(s) \\ Px(s) = u(s) \\ y(s) = Cx(s) \end{cases} \tag{3}$$

for a large set of $s_\nu = j\omega_\nu$. This may be time consuming, but can be performed off-line in a pre-computation phase. This step will be explained via examples in our experimental section.

The numerical solution of the complex boundary value problem (3) may eventually encounter numerical difficulties for frequencies ω beyond a certain high frequency limit $\overline{\omega}$. When the open-loop system has sufficient roll-off, values $G(j\omega)$ beyond $\overline{\omega}$ are usually irrelevant, but for non-sectorial systems $\bar{\omega}$ may be very large. In that case it is crucial that roll-off in $L = GK$ be generated by the controller, so that Nyquist test and H_∞-norm estimates remain reliable. Some knowledge of $\overline{\omega}$ is needed for the theoretical estimates in [3]. Note, however, that even in the difficult neutral case the limit $\overline{\omega}$ gives a much better resolution than the one we may hope to reach by approximations (E, A, B, C, D) based on finite elements or finite differences. We may also understand $\overline{\omega}$ as an indicator of up to what resolution the infinite-dimensional system may be reliably simulated. In addition to having to accept such a cut-off frequency $\overline{\omega}$, there is also the challenge to not miss resonant frequencies in the range $[0, \overline{\omega}]$ in a highly oscillatory system.

2.2. **Comments on Step 3.** A difficulty may arise in step 3 of the algorithm. Since the chosen controller structure $\mathscr{K}$ is motivated by practical considerations like implementability, simplicity, experience with distributed control architectures, it may be hard to obtain a certified initial stabilizing controller $K \in \mathscr{K}$ for G, as this has to be proved for G in infinite dimensions.

If G has only a finite number n_p of unstable poles, a finite-dimensional reduced-order approximation for stability G_r of G accurate in the unstable part is typically available. This is for instance the case for systems satisfying the spectrum decomposition condition [9, 10]. Then we may use the following heuristic: Compute a stabilizing controller $K_0 \in \mathscr{K}$ for G_r, and use the Nyquist test together with knowledge of n_p to check whether K_0 also stabilizes G. This has good chances of success in practice, [3, 7, 5, 4, 6]. Note that the requirement that G_r be accurate in the unstable part may render it useful for stabilization, but better approximations G_{perf} are typically required when performances and robustness have to be addressed.

The true difficulty in step 3 occurs if the open loop system is not sectorial and has infinitely many unstable poles, typically located in a vertical strip of the right half plane.

Then no finite-dimensional approximation G_r of G for control is available, because any such approximation has to be exact in the unstable part. Here traditional PDE control techniques may offer ways to find theoretically stabilizing control laws, which may then be used as starting points in optimization. In the case of our studies stability results are for instance [11, 12, 13, 14, 15, 16, 17, 18] for the Timoshenko beam, and [19, 20, 21, 22] for the Euler-Bernoulli beam.

Assume for instance that a simple stabilizing controller K_0 for G or $G_{\rm nl}$ based on a Lyapunov argument is known. Then we proceed as follows: We consider the stable closed loop $G_0 = (G, K_0)$ along with candidate controllers K satisfying $K_0 + K \in \mathscr{K}$. Since we have stability loop equivalence $(G, K_0 + K) \simeq ((G, K_0), K) = (G_0, K)$, we can hope to approximate $G_0 = (G, K_0)$ by a stable finite-dimensional system $G_{0,\rm stab}$, and apply the above method to the structure $\mathscr{K}' = \mathscr{K} - K_0$. If $K' \in \mathscr{K}'$ stabilizing $G_{0,\rm stab}$ is found and certified to stabilize G_0 via the Nyquist test, then $K = K' + K_0 \in \mathscr{K}$ is the solution of step 3, as it stabilizes G. For hyperbolic systems the role of the pre-stabilizer K_0 is to shift the string of vertical poles to the left half plane, from where on the frequency methods may bear.

2.3. **Comments on Step 5.** In order to perform optimization in step 5, structured controllers $K \in \mathscr{K}$ are represented by a finite set of tunable parameters, which we express by the notation $K(\mathbf{x})$ for $\mathbf{x} \in \mathbb{R}^k$. Due to non-smoothness of the H_∞-norm, program (1) is then addressed by a non-smooth optimization technique, supplemented by a method to maintain closed-loop stability of the iterates $(G, K(\mathbf{x}))$. In finite dimensions the latter may be arranged by the spectral abscissa $\alpha(A_{\rm cl})$ of the closed-loop system matrix. This takes the form of a mathematical programming constraint, $\alpha\left(A_{\rm cl}(\mathbf{x})\right) \le -\epsilon$ for some small $\epsilon > 0$, where $A_{\rm cl}(\mathbf{x})$ is the system matrix of the loop $(G, K(\mathbf{x}))$. See [23, 2]. However, this function is usually not available for infinite-dimensional plants.

In cases where a finite-dimensional approximation $G_{\rm perf}$ for performance can be used, we may follow standard lines, as now implemented in the `hinfstruct` [24, 25] and `systune` [26, 27] MATLAB functions. The optimal H_∞-controller $K^* \in \mathscr{K}$ will in the end undergo verification with the true infinite-dimensional model as in [3].

When no finite-dimensional approximation $G_{\rm perf}$ of G for control of robustness and performances is available, or when the available ones hit computationally intractable dimensions, the truly infinite-dimensional frequency domain optimization procedure of [3] is required. Here closed-loop stability of iterates is verified using the Nyquist test as explained in [3]. In addition, a repelling technique is required to prevent iterates from repeatedly trying to go outside the hidden domain of stabilizing $K(\mathbf{x})$. The fact that the Nyquist test may be brought to work here is rendered possible by the preliminary stabilization step, which gives $n_p = 0$. When initially $n_p = \infty$, we cannot use the Nyquist test. Step 5 is critical if a very large number of frequencies $s_\nu = j\omega_\nu$ is required to represent the system.

2.4. **Comment on Lyapunov stability.** When $n_p = \infty$ preliminary stabilization requires a Lyapunov function, which in PDE boundary or distributed control often derives from physical knowledge under the form of an energy functional $E(X, K)$, depending on $K \in \mathscr{K}$ and a string of parameters X. When the Lyapunov property of E can be expressed as a mathematical programming constraint $g(X, K) \le 0$, then it can in principle be included in (1). This may give rise to a more stringent stability constraint, e.g. when $g(X, K) \le 0$ implies exponential stability of the loop (G, K). However, this method is limited by the fact that in realistic situations the number of additional variables gathered in X may grossly exceed the number of truly relevant unknowns $\mathbf{x}$ in $K(\mathbf{x})$, rendering the numerical method difficult. This occurs already for finite-dimensional LTI systems, when

typically X determines a quadratic Lyapunov function $x^\top Xx$ and stability is turned into a Bilinear Matrix Inequality (BMI) $g(X,K) \preceq 0$ [28]. In that case, the number of unknown parameters in X is of the order $(n+n_K)^2$ for n the order of the system and n_K the order of K. In practice, this may lead to BMIs with several thousands of entries X, even when k the number of decision variables $\mathbf{x}$ in K stays way below 100. Choosing sparse X is not a valid option in practice, as demonstrated in [29, 30], as this leads to severe conservatism in stability, performance and robustness specifications. Furthermore, numerical testing indicates that decision variables $\mathbf{x}$ and Lyapunov variables X often differ by several orders of magnitudes, which makes BMI optimization for control highly ill-conditioned.

2.5. **Comments on Steps 6 and 7.** Simulation of the linearized system is standard when a finite-dimensional approximation is available. When $G(s)$ is computed formally or by a succession of boundary value problems, then simulation may be based on the inverse Laplace transform [31, 32].

For non-linear simulations a state-space approach is inevitable, and here a problem occurs if no finite-dimensional state-space model G_{perf} capturing the unstable part of G is available, or if the discrepancy between linear simulations based on G_{perf} and those based on G is significant. Then it will be hard to decide whether a detected instability or loss of performance is caused by non-linearity, or has numerical reasons caused by instability of the open-loop state-space model.

2.6. **Comment on stability.** For linear systems stability in the H_∞-sense is absence of unstable poles in tandem with boundedness of the closed-loop system on $j\mathbb{R}$. There is much to suggest that this is the most natural form of stability due to its physical relevance. Namely, it means that if we open the loop at two arbitrary break points w and z and add a L_2 source signal at w, then we will still receive a L_2-signal at z. For finite-dimensional systems this notion of *internal stability* implies exponential stability, but this need no longer be the case in infinite dimensions. However, we have the following quite satisfactory substitute:

Proposition 1. *Suppose the closed-loop (G,K) is H_∞-stable, K is finite-dimensional, and G is exponentially stabilizable and detectable. Then the closed loop is exponentially stable.*

Proof: This follows because K is also exponentially stabilizable and detectable, hence by Staffans [33, Lemma 8.2.7] so is the loop (G,K), and then by a result of Morris [34, Theorem 5.2], (G,K) is even exponentially stable. □

Note that exponential stabilizability and detectability may be certified with infinite-dimensional controllers which need not be practical. The analogue statement concerning strong stability is

Proposition 2. *Suppose the closed loop (G,K) is H_∞-stable, K is finite-dimensional, and G is strongly stabilizable and detectable. Then the closed loop is strongly stable.*

Proof: The proof again uses [33, Lemma 8.2.7], which guarantees that the loop (G,K) is strongly stabilizable and detectable when the components are. When the loop is H_∞-stable, we infer now using [33, Theorem 8.2.11 (ii)] that the closed loop is then also strongly stable. □

3. First study: Cantilever Timoshenko beam

Our first study uses a Timoshenko beam model [11], [35, § 5.2] of the form

$$\begin{aligned} \rho\frac{\partial^2 w}{\partial t^2} - K\frac{\partial w^2}{\partial x^2} + K\frac{\partial \phi}{\partial x} &= f \\ I_\rho\frac{\partial^2 \phi}{\partial t^2} - EI\frac{\partial^2 \phi}{\partial x^2} + K\left(\phi - \frac{\partial w}{\partial x}\right) &= g \end{aligned} \tag{4}$$

where $w(x,t)$ is the total deflection, $\phi(x,t)$ the angle of rotation, ρ the mass per unit length, I_ρ the mass moment of inertia of the cross-section, E Young's modulus, I the moment of inertia of the cross section, G the modulus of elasticity in the shear, A the cross-sectional area, k a constant depending on the shape of the beam cross-section, and $K = kGA$, all assumed constant. The right hand sides $f(x,t)$, $g(x,t)$ are used to represent external and internal damping.

The beam is clamped on the left and vibrates freely on the right, with the possibility to use feedback acting at the tip on bending moment and shear to stabilize and attenuate disturbances causing vibrations. This leads to the boundary conditions

$$\begin{aligned} w(0,t) = 0,\ \phi(0,t) &= 0 \\ K\frac{\partial w}{\partial x}(L,t) - K\phi(L,t) &= U_1(t) \\ EI\frac{\partial \phi(L,t)}{\partial x} &= U_2(t) \end{aligned} \tag{5}$$

where L is the length of the beam. Control U_1 of shear and U_2 of bending use as measured outputs the speed of rotation and distortion at the tip position

$$y_1(t) = w_t(L,t), \quad y_2(t) = \phi_t(L,t). \tag{6}$$

For the source terms we consider three scenarios, the undamped case

$$f = 0, g = 0, \tag{7}$$

external (or viscous) damping, caused for instance by friction with a surrounding medium like air resistance,

$$f(x,t) = -d_w w_t(x,t), \quad g(x,t) = -d_\phi \phi_t(x,t), \tag{8}$$

and internal, or Kelvin-Voigt, damping

$$\begin{aligned} f(x,t) &= -D_w\left(\phi_{tx}(x,t) - w_{txx}(x,t)\right), \\ g(x,t) &= -D_w\left(\phi_t(x,t) - w_{tx}(x,t)\right) + D_\phi \phi_{txx}(x,t). \end{aligned} \tag{9}$$

In the undamped case the system is unstable with infinitely many poles arranged vertically in the right half plane, so that preliminary stabilization is required to start our method. The authors of [11] show that a simple proportional control law of the form

$$U_1(t) = -\alpha w_t(L,t) + u_1(t), \quad U_2(t) = -\beta\phi_t(L,t) + u_2(t) \tag{10}$$

with $\alpha > 0$, $\beta > 0$ leads to a stable systems with new controls u_1, u_2. In the terminology of the algorithm this is the pre-stabilizing controller K_0 of step 3, and the pre-stabilized system is $G_0 = (G, K_0)$. G_0 is now amenable to our technique, which means that if a structured control law $K \in \mathscr{K}$ is sought, then we can apply the algorithm to the class $\mathscr{K}' = \{K' : \mathrm{diag}(-\alpha, -\beta) + K' \in \mathscr{K}\}$. This is used to optimize performance and robustness of the controller.

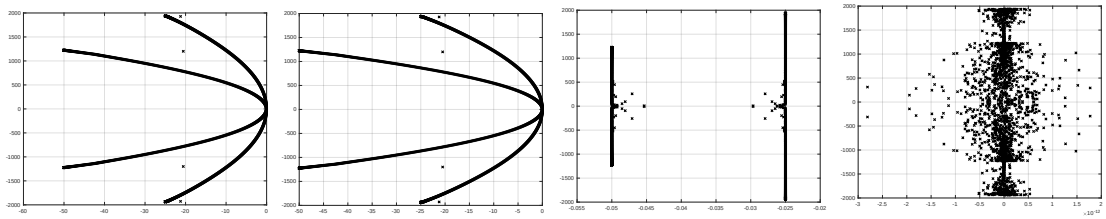

FIGURE 1. Open-loop poles of (4), (5), computed via the real-rational model G_r with $N = 500$. From left to right: both types of damping, KV-damping only, viscous damping only, no damping.

According to our general procedure the transfer function of the pre-stabilized system (4), (10) is now computed by solving a succession of elliptic boundary value problems

$$\begin{aligned} Kw'' &= \rho s^2 w + K\phi' - f \\ EI\phi'' &= I_\rho s^2 \phi + K(\phi - w') - g \\ w(0,s) &= 0, \phi(0,s) = 0 \\ Kw'(L,s) - K\phi(L,s) + \alpha s w(L,s) &= u_1(s) \\ EI\phi'(L,s) + \beta s \phi(L,s) &= u_2(s) \\ y_1(s) = sw(L,s), y_2(s) &= s\phi(L,s) \end{aligned} \tag{11}$$

which for given $s = j\omega$ has to be solved twice, with $u_1 = 1, u_2 = 0$, and $u_1 = 0, u_2 = 1$, using a solver like `bvp4c` of [36].

For the purpose of comparison and assessment of our method this potentially infinite-dimensional 2×2 transfer matrix function $G(s)$ is matched with a formally computed transfer function $G_f(s)$, which we obtain by exploiting the special structure of the Timoshenko beam system. Starting with case (7), eliminating ϕ from the Laplace transformed system (11) leads to a fourth order equation

$$w'''' = p(s)w'' + q(s)w$$

with primes denoting spatial derivatives, where in the undamped case

$$p(s) = s^2/a + s^2/b, \quad q(s) = -(s^2 + c)/b \cdot s^2/a$$

so that eigenvalues are obtained as

$$\lambda_i(s) = \pm\sqrt{\tfrac{1}{2}p(s) \pm \tfrac{1}{2}\sqrt{p(s)^2 + 4q(s)}}, \quad i = 1,2,3,4,$$

leading to $w(x,s) = \sum_{i=1}^4 A_i(s)e^{\lambda_i(s)x}$. Going back gives

$$\phi(x,s) = \frac{(c - bs^2/a)w'(x,s) + bw'''(x,s)}{s^2 + c},$$

hence $\phi(x,s) = \sum_{i=1}^4 \frac{(c-bs^2/a)\lambda_i + b\lambda_i^3}{s^2+c} A_i(s)e^{\lambda_i(s)x}$. Substituting the four boundary conditions at $x = 0$ and $x = L$ leads to a 4×4 linear system for the coefficients $A_1(s), \ldots, A_4(s)$, to be solved for every s with right hand sides $[0,0,1,0]$ and $[0,0,0,1]$. Similar computations are used for the two types of damping, where the expressions of $p(s), q(s)$ are suitably adapted.

For comparison, we also use a finite-difference approximation based on a finite-volume approach [37], which leads to a descriptor system $(E, A, B, C, 0)$. Note that straightforward finite-difference schemes fail here, as they are not stability preserving and develop spurious unstable modes for large N. Comparison of the various transfer functions are shown in Figs. 2-4.

Remark 1. Using numerical data from [11], computation of the spectrum of A shows good agreement with the results of a model analysis applied directly to the PDE. Presently the approximation $G_r = (E, A, B, C, 0)$ turns out stable, which as we know is indispensable for its use in control design. Comparison of the three ways to compute the transfer matrix are shown in Fig. 4. We observed that all methods agree over a wide range of frequencies, with deviations located in the high frequency range which, to some extent, must be taken into account when designing the controllers.

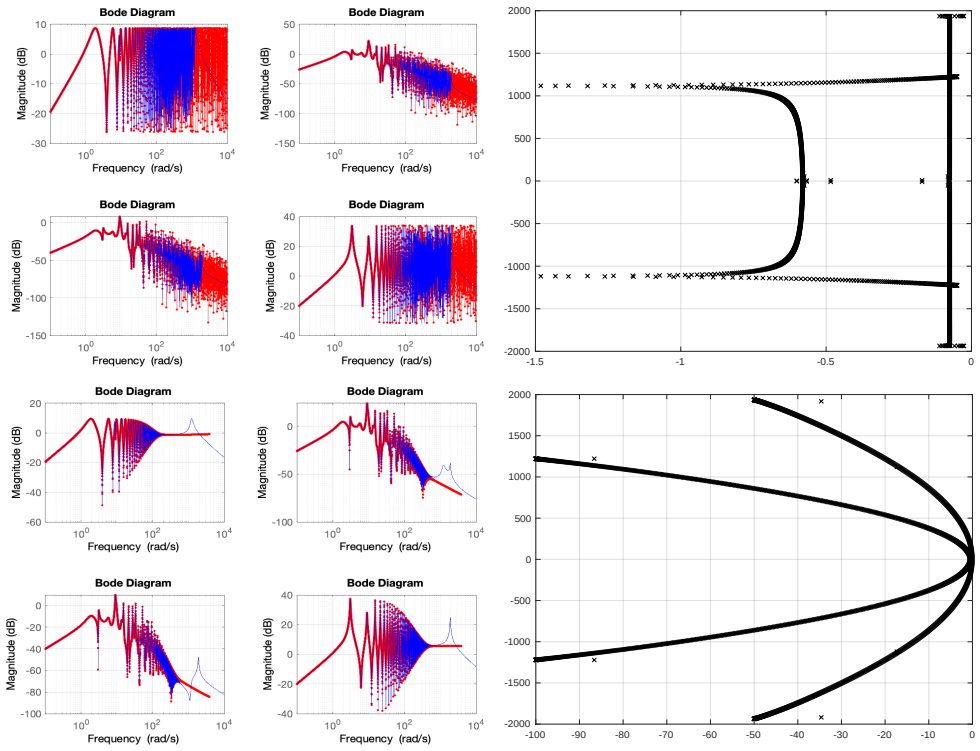

FIGURE 2. Timoshenko beam. 2×2 Bode magnitude plot. Formal method (red), finite-dimensional approximation with $N = 500$ (blue). Viscous damping (upper part) $d_w = d_\phi = 0.1$, $\alpha = 0.5, \beta = 0.1$. Closed loop spectral abscissa -0.0280. KV-damping (lower part), $D_s = D_b = 0.0002$, $\alpha = 0.5, \beta = 0.1$. Closed loop spectral abscissa -0.0487.

We end this section by addressing briefly the stability aspects. A good survey is given in [38]. The undamped case is already covered by [11], and their technique is easily seen to extend to the viscous damping case. We have the following

Proposition 3. *Let K be a finite-dimensional controller which stabilizes the Timoshenko beam G in* (4) *with boundary conditions* (5) *and no damping, or with viscous damping* (8)*, in the H_∞-sense. Then the loop (G, K) is even exponentially stable.*

Proof: It follows from [11] that G can be exponentially stabilized by the proportional control $K_0 = \text{diag}(\alpha, \beta)$ in (10), and we write $G_0 = (G, K_0)$ for the loop. The proof is given for the undamped case, but is seen to carry over to the case of a global viscous damping (8). Let $K = K' + K_0$, then we have to show that the loop $(G_0, K') \simeq (G, K_0 + K') = (G, K)$ is exponentially stable. Since K', as a finite-dimensional system, is exponentially stabilizable and detectable, it remains to prove that G_0 is exponentially stabilizable and detectable, as the result will then follows from [39] in tandem with [33, Lemma 8.2.7].

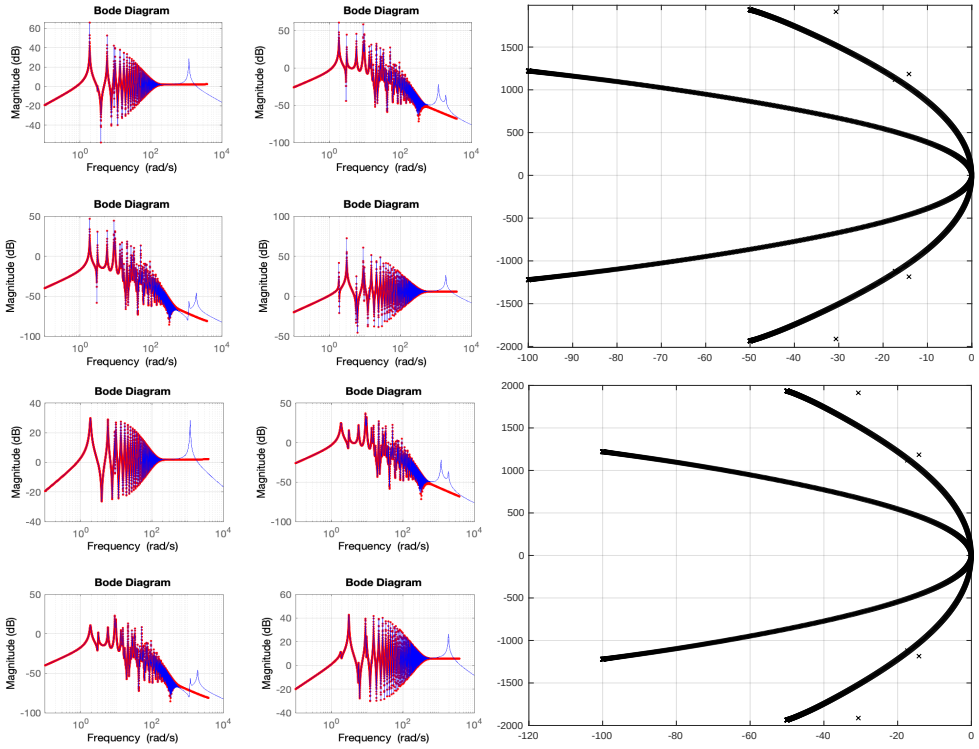

FIGURE 3. Timoshenko beam. 2×2 Bode magnitude plot. Formal method (red), finite-dimensional approximation with $N = 500$ (blue). KV damping only (upper part) $D_s = D_b = 0.0002$, $\alpha = 0, \beta = 0$. Closed loop spectral abscissa $-1.7090e-04$. KV and viscous damping (lower part) $\alpha = 0, \beta = 0$. Closed loop spectral abscissa -0.0264.

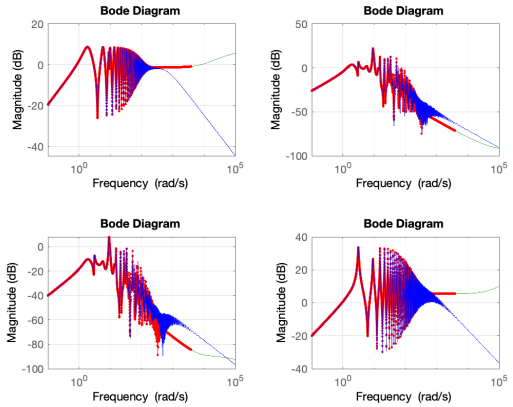

FIGURE 4. Bode magnitude plot of Kelvin-Voigt damped Timoshenko beam. Finite-dimensional approximation with $N = 100$ blue, succession of boundary value problems (green), formal method (red).

Since G_0 is exponentially stable, it is also exponentially stabilizable, so it remains to prove that G_0 is exponentially detectable. As G_0 now satisfies the spectrum decomposition assumption [9, Theorem 5.2.6], it follows from [9, Theorem 5.2.11] that in order to check exponential detectability, it suffices to show that $\ker(sI - A) \cap \ker(C) = \{0\}$, where A is the generator, C the output operator of G_0. This can be done in the frequency domain. We have to show that the system (11) with $u_1 = 0$, $u_2 = 0$ and observed outputs

$y_1(s) = sw(L,s) = 0$ and $y_2(s) = s\phi(L,s) = 0$ for every $s \in \overline{\mathbb{C}}_+$ has only the trivial solution $(w,\phi) = (0,0)$. This leads to an overdetermined linear system for the coefficients $A_1(s),\ldots,A_4(s)$, where we have to satisfy not only the boundary conditions $w(0) = 0$, $\phi(0) = 0$, $u_1 = 0$, $u_2 = 0$, but also the two conditions on the outputs $\sum_{i=1}^4 sA_i(s)e^{\lambda_i L} = 0$ and $\sum_{i=1}^4 s\frac{(c-bs^2/a)\lambda_i(s)+b\lambda_i(s)^3}{s^2+c}A_i(s)e^{\lambda_i(s)L} = 0$. These 6 conditions for the 4 unknowns can only be satisfied when $A_i(s) = 0$, $i = 1,2,3,4$. □

Stability under KV-damping is discussed in [40] and [41], where the authors allow parts of the material to be elastic, others visco-elastic, giving natural conditions under which the system is exponentially open loop stable. From the point of view of robust control design these cases represent the same level of difficulty, so in our experiments we concentrate on the case of global KV-damping, where verification by alternative methods remains easier. In this particular case, the system is guaranteed open-loop stable.

4. Second study: Cantilever Euler-Bernoulli beam

Our second study considers piezo-electric control of a thin cantilever beam, where the Euler-Bernoulli beam model may be considered adequate. As a variety of methods for this problem have been collected over the years, this is again an instance where our method can be evaluated. The equation is of the form

(12)
$$EI\frac{\partial^4 w(x,t)}{\partial x^4} + \rho A\frac{\partial^2 w(x,t)}{\partial t^2} + c_v\frac{\partial w(x,t)}{\partial t} + c_{kv}\frac{\partial^5 w(x,t)}{\partial t\partial^4 x} = K_a\left(\delta'(x-x_2) - \delta'(x-x_1)\right)u(t)$$

with boundary conditions

$$w(0,t) = 0, w_x(0,t) = 0, w_{xx}(L,t) = 0, w_{xxx}(L,t) = 0, \tag{13}$$

where L is the length of the beam, which is clamped at $x = 0$ and free at $x = L$, E is Young's modulus, I the moment of inertia of the beam, ρ its density, A the beam cross section, and where the constant K_a depends on width, thickness and piezoelectric strain constant of the actuator, with $u(t)$ representing the applied voltage. Coefficients c_v, c_{kv} stand for viscous and Kelvin-Voigt damping. The values $0 < x_1 < x_2 < L$ indicate the left and right end of the sensor/actuator pair. The measured output is

$$y(t) = K_s\left(w_x(x_2,t) - w_x(x_1,t)\right)$$

for a constant K_s now depending on properties of the sensor. The goal is to compute a finite-dimensional simply structured controller $u = Ky$ which stabilizes the structure and, in addition, allows to attenuate the induced vibrations.

While the transfer function $G(s)$ can again be computed to arbitrary precision as $G(s) = y(s)/u(s)$ by solving a succession of complex elliptic boundary value problems

$$(EI + c_{kv}s)w''''(x,s) + (\rho As^2 + c_v s)w(x,s) = K_a\left(\delta'(x-x_2) - \delta'(x-x_1)\right)u(s) \tag{14}$$

with boundary conditions

$$w(0,s) = 0, w'(x,s) = 0, w''(L,s) = 0, w'''(L,s) = 0$$

and

$$y(s) = K_s(w'(x_2,s) - w'(x_1,s)),$$

we evaluate the results using alternative ways to get $G(s)$. This includes diagonalization and expanding $G(s)$ into a series of eigenfunctions, and a classical *Ansatz* with $w(x,s) = \sum_{i=1}^4 A_i(s)e^{\lambda_i(s)}$, $\lambda_i(s)$ the eigenvalues of (14), fitting the $A_i(s)$ through the boundary conditions; see [42].

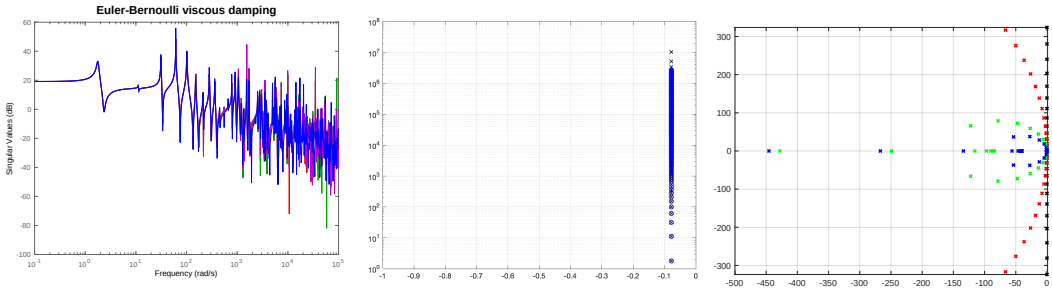

FIGURE 5. Euler-Bernoulli beam. Left: Transfer functions computed via elliptic boundary value problems (magenta), semi-formal method (red), diagonalization (green) and descriptor system (blue) ($N = 400$). Middle: Poles of descriptor system compared to theoretical poles (blue) $c_v = 0.156, c_{kv} = 0$. Right: Poles for $c_v = 0.156, c_{kv} \in \{0, 0.0001, 0.001, 0.002\}$

A finite-dimensional stability preserving approximation based on a descriptor system obtained from a finite-volume type discretization is discussed in [22]. On the right hand side we have approximated $\delta(\cdot - x_i)$ using a Gaussian $\phi(\cdot - x_i)$ centered at x_i, which gives $\delta'(\cdot - x_i)$ as $\phi'(\cdot - x_i)$. Comparisons of these transfer functions are shown in Fig. 5. Note again that the straightforward second-order difference scheme fails, as it introduces spurious modes which get unstable as $N = hL$ increases.

Realistic models for the Euler-Bernoulli beam should include damping, and in our experiment we concentrate on the viscous damping case, as from the automatic control point of view this is the severest case. As stressed in [20], design of an appropriate control law in tandem with an optimal choice of the sensor/actuator positions is the key to a successful vibration suppression in a smart structure. The authors of [20] give a good overview on previous attempts based on various controller structures such as LQG, PID or simple proportional control laws. Presently we address this problem via structured H_∞-control.

The viscous damped system is open-loop stable, [42], while stabilization of the undamped beam is for instance discussed in [43, 44, 45], where the authors use a non-realizable D-controller to stabilize the loop, which corresponds to the tip load damping of [42]. In [46] the authors use an infinite-dimensional observer.

Open-loop poles s_k of (12) are obtained from standard semi-group theory, which gives the relation

$$r_k^4 = \frac{\rho A s_k^2 + c_v s_k}{EI + c_{kv} s_k}, \quad 1 + \cos(r_k L)\cosh(r_k L) = 0$$

where the $r_k L$ are pre-computed with arbitrary precision. In tandem with [9, Thm. 5.2.6] this formula shows that the undamped Euler-Bernoulli beam cannot be exponentially stabilized by a finite-dimensional controller.

5. FEEDBACK CONTROL OF TIMOSHENKO BEAM

In this section, we discuss how a finite-dimensional controller for the Timoshenko beam can be designed. Physical parameters for (4) are chosen as

$$L = 1, \rho = 1, K = 1.5, I_\rho = 2, E = 2.5, I = 3$$

adopted from [11], where for the pre-stabilizing control (10) the values $\alpha = \beta = 0.1$ are chosen. Frequency responses of all possible combinations are shown in Fig. 12. We study the cases undamped, viscous damping ($d_w = d_\phi = 0.5$) with pre-stabilizer K_0, and Kelvin-Voigt damping ($D_s = D_b =$ 1e-4) with and without pre-stabilization. Cases with

both types of damping (fourth of Fig. 12) are the easiest and will not be treated to save space.

The design problem is formulated as a classical 2×2 reference tracking problem, where the measured outputs, shear and bending moment, should follow in a decoupled fashion reference inputs such as steps or ramps. Tracking performance requires minimizing a weighted sensitivity function $W_1(s)S(s)$, where $S = (I + GK)^{-1}$ and $W_1(s)$ is a low pass filter specifying the frequency range on which tracking should be achieved. With tracking error $e = r - y$, reference input r, and measured outputs y, this is shown in Fig. 6. Good tracking requires a high-gain W_1 at $s = 0$ to limit or eliminate errors in steady state, as well as in a range $\omega \in [0, \omega_b]$, where ω_b is the bandwidth to meet rise, settling time and overshoot constraints.

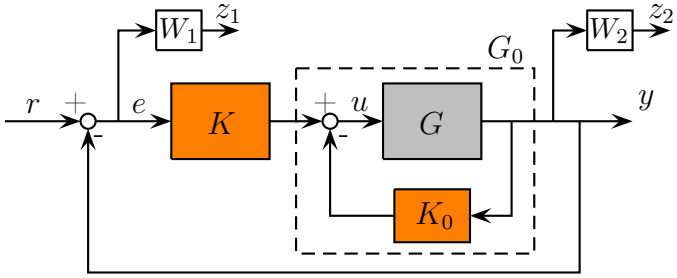

FIGURE 6. Feedback design interconnection.

In addition to tracking, the controller should also attenuate resonant modes in the high frequency range. This is addressed by minimizing the transfer function from r to y. With $y = GK(I+GK)^{-1}r$ this leads to minimizing $W_2(s)T(s)$, where $T(s) := GK(I+GK)^{-1}$ is the complementary sensitivity function and W_2 is a high-pass filter, whose role is to specify the frequency range where resonant modes are critical. Minimizing T has the additional beneficial effect to improve robustness of the design against a loss of model fidelity. As discussed in Section 3, exact and approximative methods agree at low frequencies, but significant discrepancies are observed in the high frequency range. This clearly suggests a high-pass filter W_2. Namely, minimizing T in the high frequency range then generates roll-off in the loop gain GK, thereby mitigating the effect of the infinitely many resonant high frequency modes. This also facilitates computations, both for the Nyquist stability test and for performance and robustness criteria. Further details on how the Nyquist stability can be put to work are given in [3] and references therein.

5.1. **Specific measures for the infinite dimension.** For finite-dimensional systems $G(s)$, specifications based on S and T in tandem with closed-loop stability are usually highly effective [47], especially when filters W_1, W_2 are properly chosen.

In infinite dimensions, $G(s)$ is generally only known on a finite set of sample frequencies $s_\nu = j\omega_\nu$, even though this set can potentially be enlarged and refined when required. This introduces an additional difficulty, to which we respond by adding further constraints, which we now discuss.

Putting a bound on the disk margin [48, 49, 50] is a means to prevent the Nyquist plot from getting too close to the critical point. This is expressed as $\|S\|_\infty \leq \gamma$, where $1/\gamma$ is the disk margin. This constraint has a repelling effect against stable poles crossing the imaginary axis and becoming unstable.

Two further requirements are recommended. First, one aims at realistic implementable controllers, which may be achieved by selecting classes $\mathscr{K}$ of simple low-order controllers.

For controllers $K \in \mathscr{K}$ to be practical, however, we also enforce constraints on its dynamics. This may be translated into so-called disk constraints on eigenvalues $|\lambda_i(K)| \leq \delta$, $\delta > 0$, $i = 1, \ldots, n_K$, where n_K is the order of K. More compactly, we write $\rho(K) \leq \delta$, where $\rho(.)$ denotes the spectral radius.

In the same vein, selecting sample frequencies ω_ν clearly requires minimal knowledge of the plant G, and the various methods discussed in Sections 3 and 4 should help finding suitable discretizations. As we will see later in our experiments, the choice of frequency samples must be based on the characteristics of the open-loop models and must also cope with control design constraints in programs (1) or (15) mentioned above. But even when the system G is ideally discretized, distortions may still occur outside the sets Ω. Those are referred to as *inter-sample* distortions, inherent to any discretization approach. To mitigate inter-sample effects, we propose to rule out too small damping in the controllers dynamics. This may be written as a constraint $\zeta(K) \geq \mu$, where $\zeta(.)$ is a max-function on the damping of controller eigenvalues.

Putting all those together leads to the following optimization program, which is a special case of (1):

$$\begin{array}{ll} \text{minimize} & \max\{\|W_1 S\|_{\infty,\Omega_S},\ \|W_2 T\|_{\infty,\Omega_T}\} \\ \text{subject to} & \|S\|_{\infty,\Omega_D} \leq \gamma \\ & \rho(K) \leq \delta \\ & \zeta(K) \geq \mu \\ & K \in \mathscr{K} \text{ stabilizes } G \end{array} \tag{15}$$

Here $\|M(s)\|_{\infty,\Omega}$ is short for $\max_{\omega\in\Omega} \max_i \sigma_i(M(j\omega))$ with σ_i denoting singular values. Sample frequencies Ω_S, Ω_T are adapted to $W_1 S$ and $W_2 T$, Ω_D is adapted to the disk margin constraint, and sampling Ω_N to the Nyquist test. This gives extra flexibility and can be exploited to reduce execution times and to address specific frequency bands.

Program (15) is solved using nonsmooth bundle or trust region optimization techniques, [51, 7, 52, 53, 8]. However, a new element is required for infinite-dimensional closed-loop stability. In finite dimensions this may be assured by a constraint $\alpha(A_{cl}(K)) \leq -\epsilon$ on the closed-loop spectral abscissa. In infinite dimension, particularly for non-sectorial systems, this in no longer possible, as $\alpha(A_{cl})$ is not reliably computable. Instead we use a workaround based on the Nyquist stability criterion, which we now explain.

As soon as G is pre-stabilized, closed-loop stability is maintained during optimization over $K \in \mathscr{K}$ by keeping the winding number of $f(s) = \det(I + G(s)K(s))$ at the correct value. This requires that the number of unstable poles of iterates $K \in \mathscr{K}$ does not change either. Presently this is assured since the damping constraint $\zeta(K) \geq \mu$ restricts the search $K \in \mathscr{K}$ to stable controllers $\alpha(K) < 0$, which means that the correct winding number for closed-loop stability is 0. As soon as a step $K^+ = K + dK$ leads to an unstable loop, recognized by a non-zero winding number, backtracking $K^+ = K + \alpha dK$, $0 < \alpha < 1$, or tightening proximity control, are used to maintain stability. In the next step it is then necessary to prevent the optimizer from tempting the direction dK again. As a rule this may be achieved by using the closed-loop sensitivity function as a barrier, as has been pointed out in [3]. One has just to be aware that $\|S(K)\|_\infty$, while having a large peak at points K where the closed-loop turns unstable, may show misleading small values for points K^+ farther beyond the point of instability, so does not behave in the same way as say a log-barrier function. Our experiments indicate that this difficulty is avoided through the combined use of the barrier and the Nyquist test.

The Nyquist test gives a stability certificate as soon as it can be proved that between two sample frequencies ω_ν and $\omega_{\nu+1}$, the closed curve γ_ν obtained by concatenating the true Nyquist arc $\{f(\omega) : \omega \in [\omega_\nu, \omega_{\nu+1}]\}$ with the segment $[f(\omega_{\nu+1}), f(\omega_\nu)]$ does not encircle

the origin. This can for instance be arranged when a prior bound on the variation $f'(\omega)$ of $f(\omega) = \det(I + K(j\omega)G(j\omega))$ can be provided. We call a function $L[\omega^-, \omega^+]$ a first-order bound if $L[\omega^-, \omega^+] \geq |f'(\omega)|$ for all $\omega \in [\omega^-, \omega^+]$. Then any sampling ω_ν satisfying $L[\omega_\nu, \omega_{\nu+1}](\omega_{\nu+1} - \omega_\nu) \leq |f(\omega_\nu)| + |f(\omega_{\nu+1})|$ gives a provable certificate of stability via the Nyquist test. See [3, Lemma 3], and Algorithm 1 of that reference how to construct the ω_ν. Even when no rigorous bound $L[\cdot, \cdot]$ is available, numerical bounds usually give excellent results. Note that the bound comes into play only for those parts of the Nyquist contour which are relatively close to the origin.

The Nyquist test has precedence over all other functions in (15). Clearly, objectives and constraints need not be computed when the Nyquist test fails at $K^+ = K + dK$, which speeds up computations.

Appropriate sampling with certificate Ω_S, Ω_T and Ω_D for W_1S, W_2T and S required for the constraints and max objective of (15) is also described in [3, Lemma 3]. We also write Ω_N for sampling for the Nyquist criterion. In practice, it makes sense to take the same sampling grid $\Omega_N = \Omega_D$, because the disk margin and the Nyquist test are equivalent measures of singularity, that is, $\underline{\sigma}(S(j\omega)^{-1}) = \underline{\sigma}(I + G(j\omega)K(j\omega)) = 0$ if and only if $\det(I + G(j\omega)K(j\omega)) = 0$.

Note that undersampling Ω_S and Ω_T may lead to underestimating the values of the H_∞-norms in the cost function of (15), but is less critical than undersampling Ω_N, which may put stability at stake.

In our experiments, we have adopted two strategies to deal with the beam tracking problem. The first one is based on deriving a reduced-order approximation of the beam dynamics giving a descriptor state-space model (E, A, B, C, D). The second uses the idea of [3], which avoids approximations and relies on frequency domain data of the beam obtained from (11). This is more in line with data-driven control techniques [54, 55, 56], even though we have the possibility to supplement additional data if required. It leads to sampled data $\{G(j\omega) : \omega \in \Omega\}$ for a finite $\Omega \subset [0, \infty]$. Both strategies have been discussed in Section 2.

5.2. **Undamped Timoshenko beam.** We start with the case of the undamped Timoshenko beam, which is certainly the most challenging, numerically and in terms of feedback design. A reduced-order model retaining 20 resonant modes, that is, of order 40 and exact data are compared in Fig. 7 left. These models $(E, A, B, C, 0)$ and $\{G(j\omega) : \omega \in \Omega\}$ essentially differ in the high frequency range, where the reduced-order model disregards resonant modes.

Good tracking and decoupling properties would dictate using integral action in the controller. This is not possible here, however, because measurements are of derivative type. In response we use a pseudo-integrator $1/(s+\varepsilon)$, directly included into the structure of the controller as $K := 1/(s + \varepsilon)\widetilde{K}$, where $\widetilde{K}$ is the optimized portion, while $\varepsilon =$ 1e-3 remains fixed. This can also be directly embedded into the cast (15) by the substitutions $G \leftarrow G/(s+\varepsilon)$. Constraints on K now turn into constraints on $\widetilde{K}$. As structural constraint we choose $\widetilde{K} \in \mathscr{K}_8$, the set of 8th-order controllers, a choice motivated by preliminary testing. This leaves 54 tunable parameters or optimization variables $\mathbf{x}$ corresponding to tridiagonal state-space realizations. Those realizations do not limit generality and are less costly than full state-space forms. Note that including a pseudo-integrator which plays the role of a pre-compensator into the plant G is reminiscent of the loopshaping approach [57, 58].

Designs based on a reduced-order state-space model and on the infinite-dimensional model use the same cast (15) to allow comparison. With a state-space model G, program

(15) can be solved using `systune` [26, 59, 60], whereas its data-based variant has to rely on the more recent technique in [3].

Weightings for tracking W_1 and roll-off W_2 shown in Fig. 7 middle are

$$W_1(s) := \frac{0.05s + 0.9987}{s + 0.0009987}, \qquad W_2(s) := \frac{1000s + 2}{s + 2000}.$$

A disk margin of $1/\gamma$ with $\gamma = 0.7$ is specified, which leads to the constraint $\|S\|_\infty \leq 1/0.7$. Due to plant zeros at the origin, it is not possible to minimize the sensitivity function S at the zero frequency. The H_∞ norm $\|W_1 S\|_\infty$ in (15) is therefore restricted to the frequency band $[10^{-3}, \infty)$.

The controller radius constraint in (15) is set to $\delta = 100$. Its minimal damping is set to $\mu = 10^{-2}$. Taken together with the order limit $\widetilde{K} \in \mathscr{K}_8$ these constraints secure practical and implementable controllers.

Design (15) based on frequency-domain data has to trade accuracy against execution times. Frequency-domain sampling a system with an infinite number of resonances as in Fig. 7 may seem daunting, because peak frequencies will almost certainly be missed. As an example, 1e4 points were used to plot Fig. 7, and some plots in Sections 3 and 4 required even more points. In fact, as far as stability is concerned, it is sufficient to increase the sampling density only in those frequency ranges where the controller gain is significant. Clearly, frequency ranges where the loop gain GK is small do not contribute much to the Nyquist stability criterion, as there $\det(I+GK) \approx 1$. This is easily devised by taking into account the dynamics of the beam in Fig. 7 along with the design constraints.

In the present application, we distinguish 3 frequency intervals for the disk margin, $\Omega_D = \Omega'_D \cup \Omega''_D \cup \Omega'''_D$ in (15) and $\Omega_N := \Omega_D$ for the Nyquist criterion. In the low frequency range $\Omega'_D =$ [1e-8, 1] rad/s, we have high gain control but dynamics are rigid, thus 300 linearly spaced samples suffice. In the mid frequency (crossover) range $\Omega''_D = [1, 15]$, we have moderate gain control but resonant dynamics and it is enough to use 500 samples. For higher frequencies $\Omega'''_D = [15,$ 1e3], we have low roll-off control with resonant dynamics. We therefore cut down density to only 100 samples. These figures convey the general idea that is followed repeatedly in the sequel.

Remark 2. In order to apply the certificates in [3], it is necessary to adapt the sampling grids $\Omega_S, \Omega_T, \Omega_D, \Omega_N$ not only to G, but also to the controller K. Since K changes during optimization, this could appear to be a major difficulty due to a large number of updates. Theoretically this can be avoided by considering optimization with inexact data [61], or by fixing the grid and re-checking the result in the end, using re-starts if the grid turned out insufficient.

Fortunately, this is more a theoretical quest than a challenge in practice, as updates due to varying K are rare. Presently we never had to stop-and-restart (15) with refined sampling.

More significantly, it can be observed that running times fall from 2 hours for blind sampling with 1e5 nodes to less than 2 minutes using the outlined strategy.

As mentioned earlier, soft objectives in (15) do not necessarily require very dense sampling. In this application, we have used a linear spacing of 1e3 frequencies over the range $\Omega_S =$ [1e-3, 1e2] for tracking and $\Omega_T =$ [1e-1, 1e3] for roll-off.

Reduced-order model $G_r = (E, A, B, C, 0)$, controller K_r obtained from G_r, full frequency data model G and controller K obtained through G are compared in Fig. 7. For K_r and K, high gain is observed at low frequencies, low gain at high frequencies, as required for good performance and roll-off, respectively. Multivariable Nyquist plots associated with the reduced-order model and the infinite-dimensional model are shown in Figs. 8 and 10. Stability is confirmed in all cases with zero winding numbers as required.

We observe little differences between the two approaches, despite the relatively low order of the state-space model, which may be attributed to the roll-off effect introduced by the controller. Step response simulations in a similar configuration are displayed in Figs. 9 and 11 and indicate good agreement in terms of rise time and decoupling.

Simulations for the infinite-dimensional model were obtained using numerical Laplace inversion based on the conventional Bromwich contour. Talbot's idea of using deformed contours [62, 31] is not exploited, but we noticed that shifting the Bromwich contour along the x-axis, while preserving analyticity, can help improving accuracy.

Finally, it appears that both strategies compete on equal terms in this example. Stability, performance and robustness are nearly indistinguishable. A major advantage of the direct frequency-domain approach being that the critical phase of devising a suitable reduced-order model along with post-certification in infinite dimension are entirely bypassed. We will therefore favor this approach in the next applications.

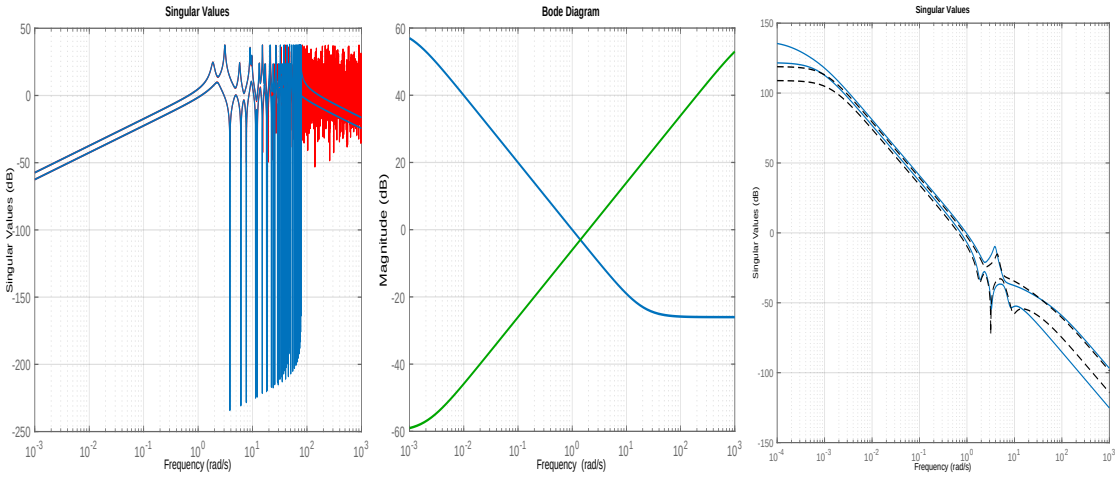

FIGURE 7. Undamped Timoshenko beam. Left: singular values of infinite-dimensional model G and reduced LTI model G_r of order 40. Middle: weighting functions used in (15). Right: singular values of controllers K_r based on reduced-order model (solid), and K based on infinite-dimensional-model (dashed).

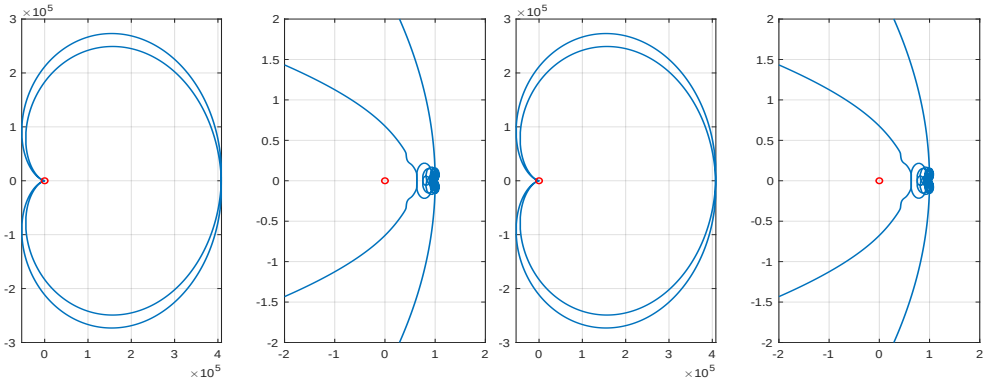

FIGURE 8. Undamped Timoshenko beam. Multivariable Nyquist for reduced-order design. Two left: reduced-order model. Two right: infinite-dimensional model. Critical point, red dot, at the origin.

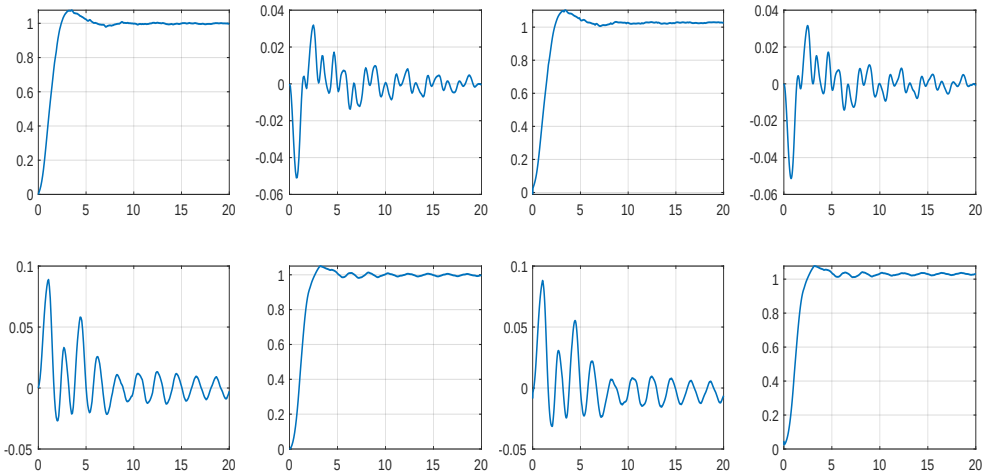

FIGURE 9. Undamped Timoshenko beam. Closed-loop step responses with controller based on reduced-order model. Two columns left: reduced-order model. Two columns right: infinite-dimensional model

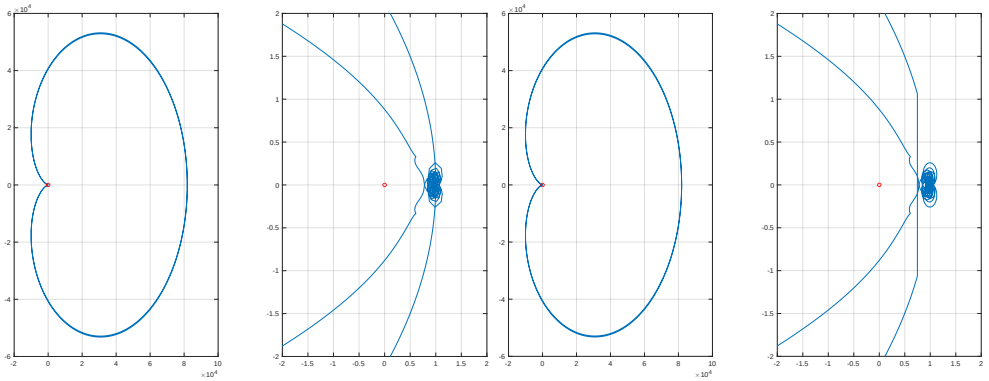

FIGURE 10. Undamped Timoshenko beam. Multivariable Nyquist for infinite-dimensional design. Two left: infinite-dimensional model. Two right: reduced-order model.

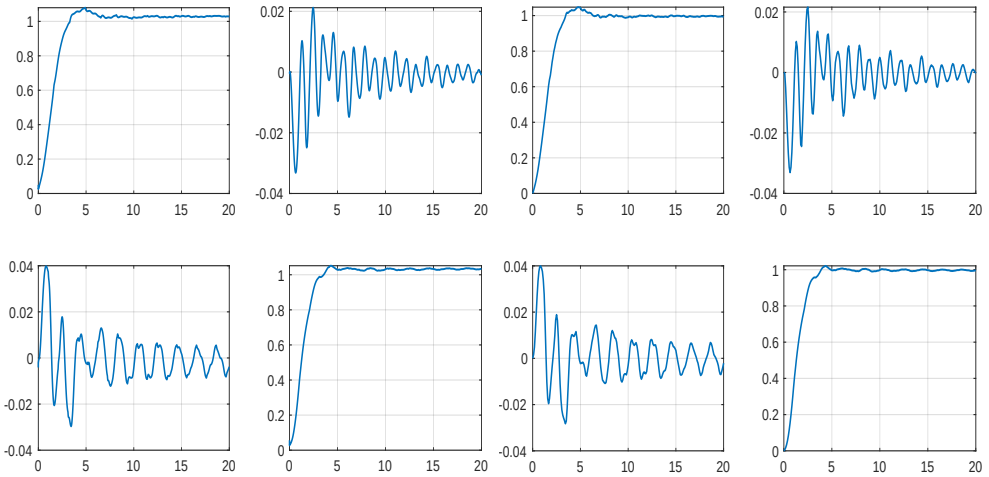

FIGURE 11. Undamped Timoshenko beam. Closed-loop simulations for infinite-dimensional design. Two columns left: infinite-dimensional model. Two columns right: reduced-order model.

5.3. **Timoshenko beam with damping.** In this section, we consider the Timoshenko beam with two types of damping, viscous, Kelvin-Voigt, and both together. Frequency responses of the beam are shown in Fig. 12.

It is observed that viscous damping preserves the hyperbolic pole pattern of the undamped case. The difference is that resonances are significantly attenuated, in our example by a factor of 10 dB when the pre-stabilizer K_0 is on and 30 dB otherwise. This is related to a uniform pole shift in the left half plane, see Section 3. With Kelvin-Voigt damping, the hyperbolic pattern disappears, and poles in the left half plane take a parabolic form. Peaks fade out with increasing frequencies and vanish beyond 1e3 rad/s. High frequency modes are much more damped than lower ones. See also Section 3. With both viscous and Kelvin-Voigt damping a combination of both effects are observed in the pole pattern.

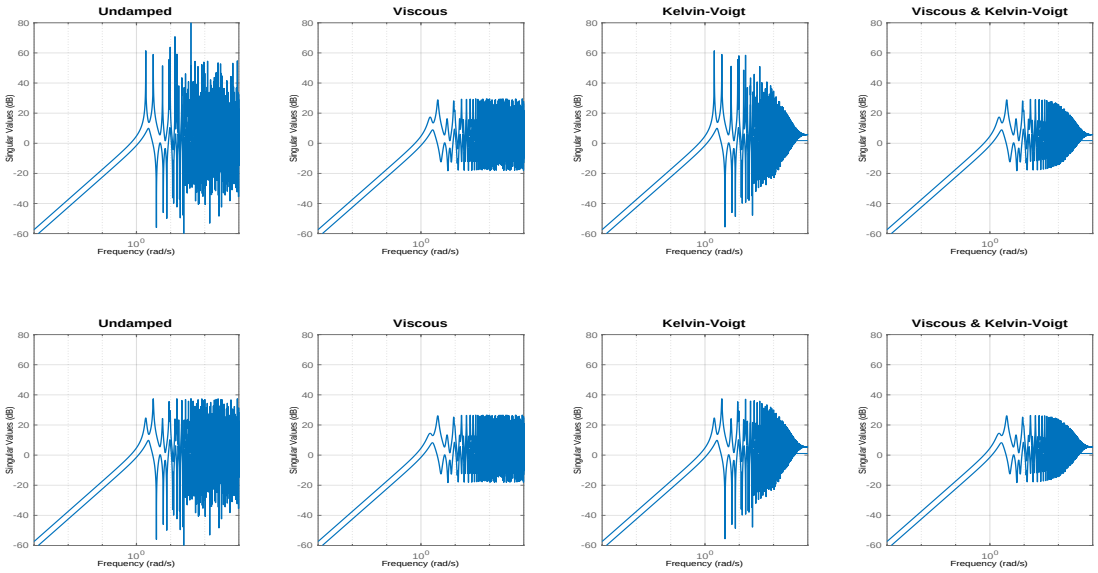

FIGURE 12. Timoshenko beam. First row: without pre-stabilizer. Second row: with pre-stabilizer K_0. From left to right: Undamped, viscous alone, Kelvin-Voigt alone, viscous and Kelvin-Voigt.

5.3.1. *Kelvin-Voigt damping with pre-stabilizer.* We consider Kelvin-Voigt damping alone and re-use Program (15) without change, because the low frequency peaks are identical to those of the undamped case. Results are shown in Fig. 13. Similarly to the undamped case, strong roll-off is achieved for $\omega > 1$ rad/s with notch filtering of low frequency resonances. Good rise times are attained with no more than 4% coupling of the responses.

5.3.2. *Kelvin-Voigt damping without pre-stabilizer.* Comparing frequency responses in the 3rd column of Fig. 12, we see that resonances are amplified by 30 dB when the pre-stabilizer is off. This leads now to a much more complicated design problem, which requires a review of objectives and constraints, the challenge being to enable the Nyquist test during optimization. The cut-off frequency of performance weight W_1 was reduced from 1 to 0.5 rad/s. For the roll-off weight W_2, we specified an attenuation of 15 dB at 1.88 rad/s corresponding to the 1st resonant mode. This lead to

$$W_1(s) := \frac{0.05s + 0.4994}{s + 0.0004994}, \qquad W_2(s) := \frac{1000s + 0.3343}{s + 334.3}.$$

The changes, however, proved insufficient, as bending of poles to parabolic shape in Fig. 3 is fairly weak for the chosen c_{kv}. It was necessary to increase the order of the

controller from 8 to 10 for $\widetilde{K}$, leading to the structure $K := 1/(s+\epsilon)\widetilde{K}$ with $\widetilde{K} \in \mathscr{K}_{10}$. Also, the disk margin requirement in (15) had to be alleviated from 0.8 to 0.7 which is equivalent to setting $\gamma = 1/0.7$ in program (15). Results are consistent with what we had obtained so far except that lower quality performances are achieved. See Fig. 14.

5.3.3. *Viscous damping alone.* For viscous damping, frequency responses in Fig. 12 suggest that better performance can be achieved. This is easily assessed by applying simple changes to the performance filter W_1. The DC gain of the filter is increased from 1e3 to 3.1623e3 corresponding to 10 dB amplification. Its cut-off frequency at 0 dB is increased from 1 to 1.3 rad/s. Running again program (15) with the other constraints untouched leads to the results in Fig. 15. The Nyquist criterion certifies exponential stability, based on Proposition 1. The improvement in the rise time is from about 4 sec. (undamped and Kelvin-Voigt damping) to 2 sec. with viscous damping $d_w = d_\phi = 0.5$. Better decoupling is also obtained.

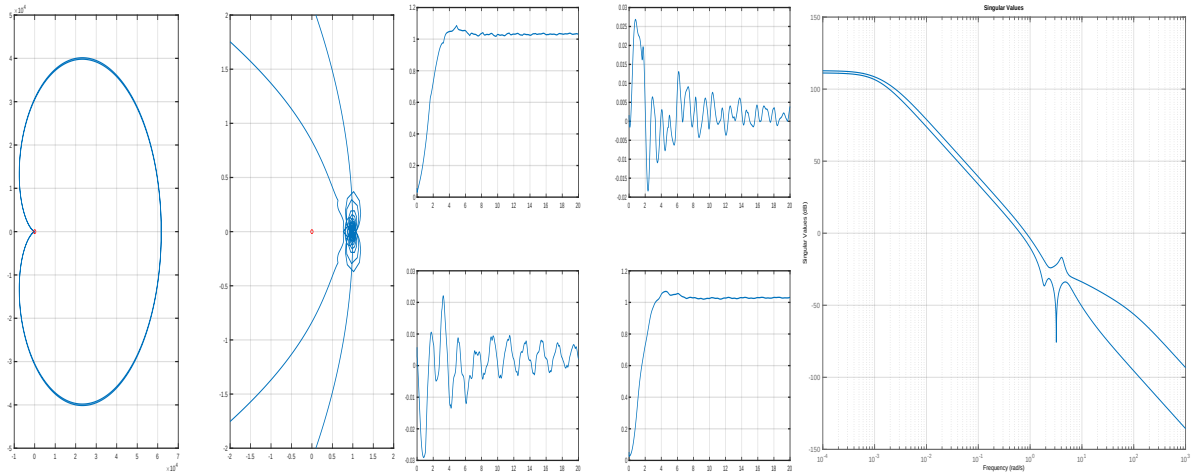

FIGURE 13. Timoshenko beam with Kelvin-Voigt damping alone and pre-stabilizer. Two left: Nyquist plot. Middle: step responses. Right: singular value plot of controller.

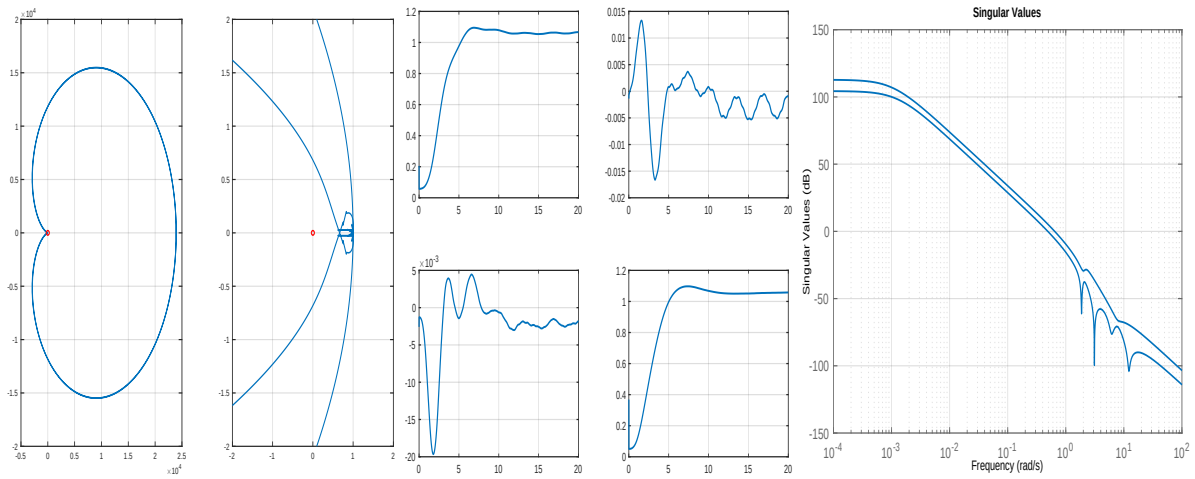

FIGURE 14. Timoshenko beam with Kelvin-Voigt damping and no pre-stabilizer. Two left: Nyquist plot. Middle: step responses. Right: singular value plot of controller.

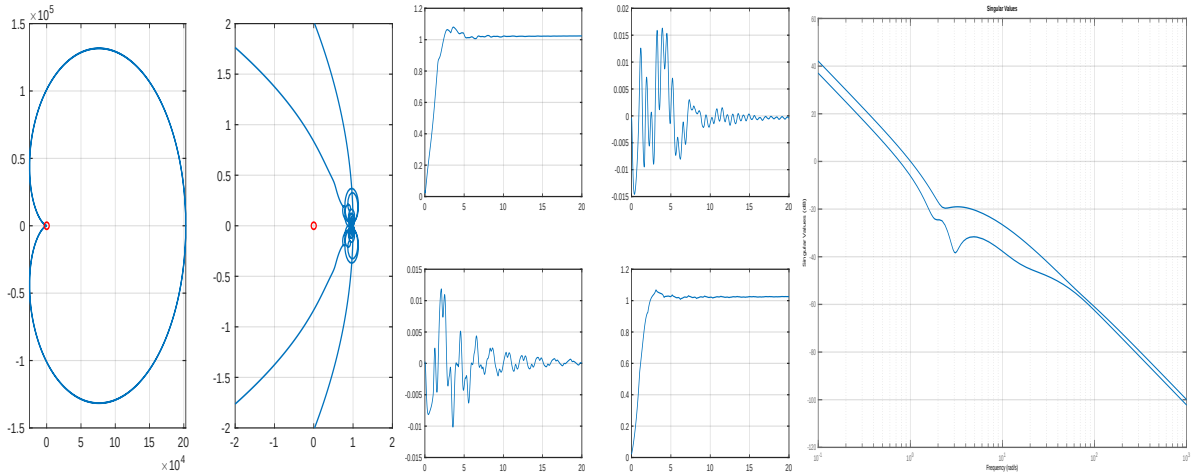

FIGURE 15. Timoshenko beam with viscous damping alone. Two left: Nyquist plot. Middle: step responses. Right: singular value plot of controller.

6. Feedback control of Euler-Bernoulli beam

Much the same approach is considered for the Euler-Bernoulli beam. We capitalize on previous results and use the method based on the infinite-dimensional model. The formulation is now a SISO tracking problem. The cast (15) is unchanged in terms of (γ, δ, μ), whereas the weighting filters in the objective function require adjustment. All models were computed by solving complex elliptic boundary value problems (14) as in Sections 2-4.

6.1. **Viscous damping alone.** We study the case of a strong viscous damping $c_v = 0.5079$ alone. The Euler-Bernoulli model is to some extent less realistic and exhibits resonant modes at higher frequencies, see Fig. 16 left and middle. Clearly, this can be exploited to achieve a larger bandwidth and therefore better performance. Weights are shown in Fig. 16 middle with transfer functions:

$$W_1(s) := \frac{0.001s + 2}{s + 0.002}, \qquad W_1(s) := \frac{1000s + 6}{s + 6000}.$$

Note that W_1 specifies a bandwidth of 2 rad/s, which corresponds approximately to a settling time of 1.5 seconds. Filter W_2 reflects a roll-off constraint with crossover at 6 rad/s.

Solving (15) over $K \in \mathscr{K}_5$, the set of 5th-order controllers, gives the controller with Bode diagrams in Fig. 16 right and transfer function:

$$K(s) := \frac{-0.0144s^4 - 0.3585s^3 - 54.58s^2 - 9.669s - 173.8}{s^5 + 16.9s^4 + 106.1s^3 + 108.1s^2 + 539.7s + 3.678}.$$

Closed-loop stability is checked using the Nyquist criterion in Fig. 17. Open- and closed-loop simulations are compared in the third and fourth plots of Fig. 17. Results all agree with the design constraints. As before, program (15) was solved with $\Omega_D = \Omega'_D \cup \Omega''_D \cup \Omega'''_D$ and $\Omega_N := \Omega_D$ for the Nyquist criterion. We have used 250 samples in the low frequency range $\Omega'_D =$ [1e-1, 1] rad/s, 200 samples in the mid frequency range $\Omega''_D = [1, 6]$ and 500 samples in $\Omega'''_D = [6, 1e3]$. For Ω_S and Ω_T, we have used 1e3 frequencies over the range [1e-1, $1e3$].

6.2. **Kelvin-Voigt damping.** In this last study, we return to the cases discussed in Section 4 and displayed in Fig. 5. We have moderate viscous damping $c_v = 0.156$ and

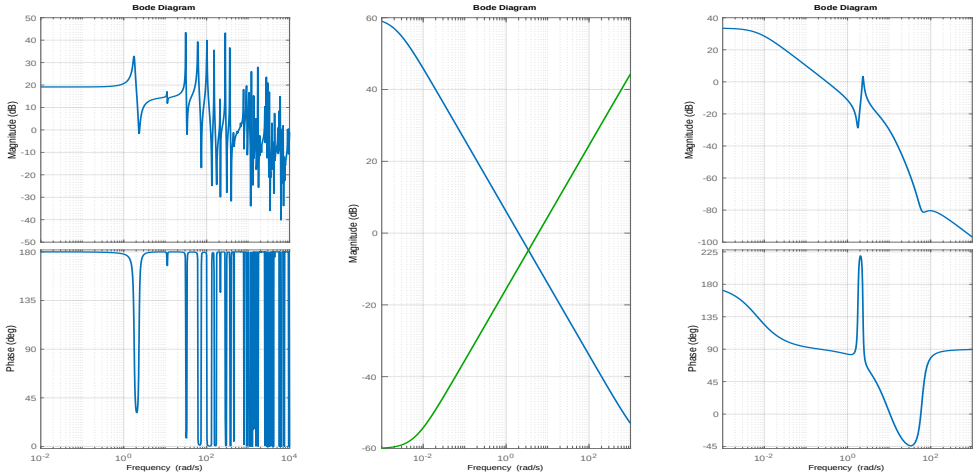

FIGURE 16. Euler-Bernoulli beam. Left: Bode diagram of infinite-dimensional system. Middle: weighting functions used in program (15). Right: Bode gain and phase diagrams of optimized controller.

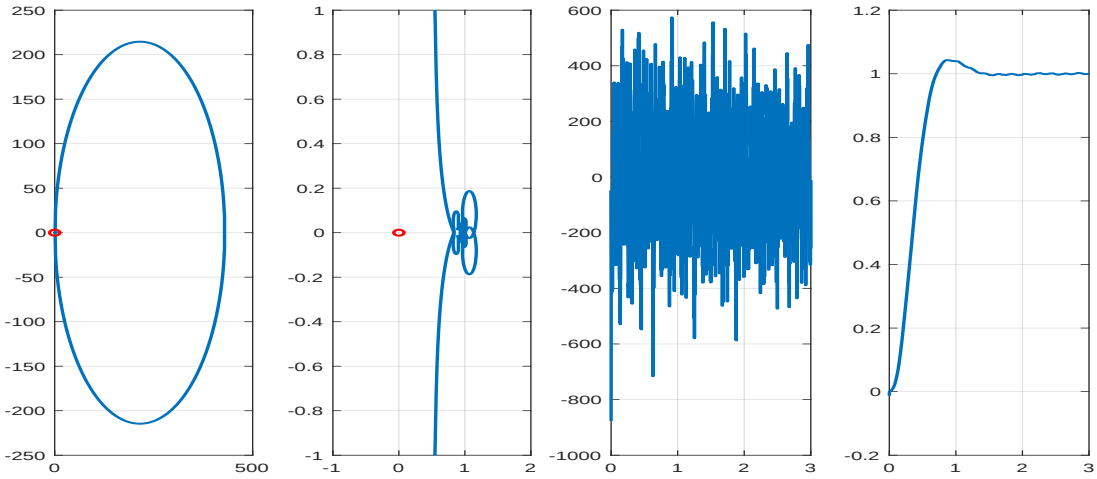

FIGURE 17. Euler-Bernoulli beam. Two leftmost: Nyquist plot. Third: Open-loop step response. Right: Closed-loop step response.

Kelvin-Voigt dampings $c_{kv} \in \{0, 1\text{e-}3, 2\text{e-}3\}$. For the 3 cases, the first resonant mode appears around 0.5 rad/s. Performance requirements should therefore be reduced. The cutoff frequencies at 0 dB are set to 0.5 and 1 rad/s for W_1 and W_2, respectively. Running program (15) for all 3 cases leads to the results shown in Fig. 18. As before, stability is assessed through Nyquist plots. We observe in the 3rd column that open-loop step responses vary widely with the Kelvin-Voigt damping. The undamped case $c_{kv} = 0$, middle plot, exhibits almost persistent oscillations. This is consistent with the pole pattern in the right plot of Fig. 5. Step responses in closed loop (right plots) are however very similar. This is due to the fact that the pole pattern in Fig. 5 match in a low frequency horizontal band $[-10, 10]$ rad/s. This confirms, if such confirmation is still needed, that low frequency resonances are the main limiting factor in feedback tracking problems regardless of pole asymptotics. Controllers computed in this study are simple state-space systems of order 5 and are available upon request. We note that our approach is a major progress over existing procedures, which either use PDE control techniques,

where optimizing K is impossible or controller structures are impractical, or rely on low-order approximations such as finite elements, where high order dynamics are typically ignored.

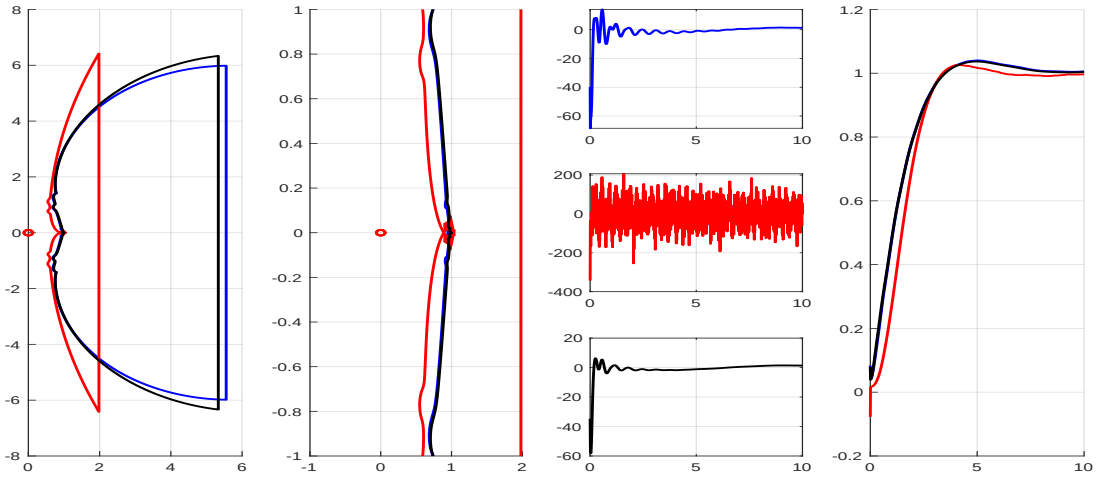

FIGURE 18. Euler-Bernoulli beam. Viscous damping $c_v = 0.156$, Kelvin-Voigt dampings $c_{kv} \in \{0, 1\text{e-}3, 2\text{e-}3\}$ with colors red, blue and black. Two leftmost: Nyquist plots. Third column: Open-loop step responses. Right: Closed-loop step responses.

7. Conclusion

The main purpose of this note was to investigate whether, or to what extent, H_∞-control methods remain applicable in open loop systems with an infinity of open loop poles arranged in vertical strips close to the imaginary axis. This challenging situation occurs when models include hyperbolic PDEs, or in neutral systems. It may be considered unrealistic or non-physical, because such systems have no natural roll-off and respond substantially to arbitrary high frequency stimuli. This extremal behavior is to some degree defanged when sensor and actuator models are included, or when damping is added to make models more realistic. We studied these effects exemplarily for a cantilever Timoshenko and an Euler-Bernoulli beam, where undamped or viscous damped systems exhibit such non-sectorial pole pattern, while Kelvin-Voigt damping bends poles to a more realistic sectorial shape. Surprisingly, our methods prove effective even in the challenging neutral case. We synthesize finite-dimensional implementable H_∞-controllers, which attenuate high frequency stimuli in closed loop, introduce realistic roll-off, and still act sufficiently fast, as required in a technically feasible controlled system. Synthesis is based on a recent infinite-dimensional frequency-based optimization technique.

On closer look the question whether, or to what extent, the infinite dimension of G hampers the choice of synthesis strategies, calling for elements one would not be inclined to consider in a reduced-order model, has the following partial answer.

We had to enforce significant disk margins in closed loop, constraints on the dynamics of $K \in \mathscr{K}$ and suitable roll-off in the high-frequency range in order to enable the Nyquist test during optimization and to make our frequency-domain approach more reliable. This restricts the set of reachable controllers to some extent. However, in the present beam studies this type of constraint did not seem totally unnatural and might be opportune even in reduced-order models. Specifically, disk margins improve robustness

of the loop and roll-off constraints attenuate measurement noise and high-frequency resonances. Constraints on K, on the other hand, are less conventional and are tied to our frequency sampling technique.

A more severe restriction occurred in the Timoshenko study when the pre-stabilizer K_0 was not available, as then the lack of roll-off in the system strongly limited the choice of the synthesis strategy (see Section 5.3.2, and to a lesser degree, Section 6.2). Altogether, this quest may require further investigation with other non-sectorial open-loop models. A difficulty in the assessment is that in the literature comparison with finite element or reduced-order synthesis, where these restrictions might not be on the agenda, often disregards high frequency effects of the final controllers, by conducting simulations within the reduced-order beam models only.

A detail to be mentioned is that in beam models velocity measurements seem to alleviate functional analytic Lyapunov-based proofs for stabilization, but render synthesis harder from a practical control point of view, as e.g. integral action and low frequency high gain for good tracking are impeded.

Finally, the frequency-domain approach taken in this work offers a myriad of possible extensions including the design of two-degree-of-freedom or multi-block controllers, as well as of controllers dealing with robustness against parameter uncertainties or self-adjusting to variations in PDE dynamics.

References

[1] Pierre Apkarian and Dominikus Noll. Optimization-based control design techniques and tools. In J. Baillieul and T. Samad, editors, *Encyclopedia of Systems and Control*. Springer-Verlag, 2015.

[2] Jim V. Burke and Michael L. Overton. Differential properties of the spectral abscissa and the spectral radius for analytic matrix-valued mappings. *Nonlinear Anal.*, 23(4):467–488, 1994.

[3] Pierre Apkarian and Dominikus Noll. Structured H_∞-control of infinite-dimensional systems. *International Journal of Robust and Nonlinear Control*, 28(9):3212–3238, 2018.

[4] Pierre Apkarian and Dominikus Noll. Boundary control of partial differential equations using frequency domain optimization techniques. *Systems & Control Letters*, 135:104577, 2020.

[5] Pierre Apkarian and Dominikus Noll. Boundary feedback control of an anti-stable wave equation. *IMA Journal of Mathematical Control and Information*, 37(4):1367–1399, 2020.

[6] Pierre Apkarian and Dominikus Noll. Mixed L_1/H_∞-synthesis for L_∞-stability. *International Journal of Robust and Nonlinear Control*, 32(4):2119–2142, 2022.

[7] Pierre Apkarian, Dominikus Noll, and Laleh Ravanbod. Non-smooth optimization for robust control of infinite-dimensional systems. *Set-Valued Var. Anal.*, 26(2):405–429, 2017.

[8] Dominikus Noll. Cutting plane oracles to minimize non-smooth non-convex functions. *Set-Valued Var. Anal.*, 18(3-4):531–568,2010.

[9] Ruth F. Curtain and Hans Zwart. *An Introduction to Infinite-Dimensional Linear Systems Theory*, volume 21 of *Texts in Applied Mathematics*. Springer-Verlag, 1995.

[10] Klaus-Jochen Engel and Rainer Nagel. *One-Parameter Semigroups for Linear Evolution Equations*. Graduate Texts in Math. Springer, 2000.

[11] Jong Uhn Kim and Yuriko Renardy. Boundary control of the Timoshenko beam. *SIAM Journal on Control and Optimization*, 25(6):1417–1429, 1987.

[12] Kangsheng Liu, Shuping Chen, and Zhuangyi Liu. Spectrum and stability for elastic systems with global or local Kelvin–Voigt damping. *SIAM Journal on Applied Mathematics*, 59(2):651–668, 1998.

[13] Xinhong Tian and Qiong Zhang. Stability of a Timoshenko system with local Kelvin–Voigt damping. *Zeitschrift für angewandte Mathematik und Physik*, 68(1):1–15, 2017.

[14] Denis Mercier and Virginie Régnier. Non uniform stability for the Timoshenko beam with tip load. *arXiv preprint arXiv:1507.00445*, 2015.

[15] Chris Guiver and Mark R Opmeer. Non-dissipative boundary feedback for Rayleigh and Timoshenko beams. *Systems & Control Letters*, 59(9):578–586, 2010.

[16] Amin Mehrvarz, Hassan Salarieh, Aria Alasty, and Ramin Vatankhah. Vibration boundary control of Timoshenko micro-cantilever beam using piezoelectric actuators. *Scientia Iranica*, 25(2):711–720, 2018.

[17] Ömer Morgül. Dynamic boundary control of the Timoshenko beam. *Automatica*, 28(6):1255–1260, 1992.
[18] Marié Grobbelaar-Van Dalsen. Uniform stability for the Timoshenko beam with tip load. *Journal of Mathematical Analysis and Applications*, 361(2):392–400, 2010.
[19] Kais Ammari and Marius Tucsnak. Stabilization of Bernoulli–Euler beams by means of a pointwise feedback force. *SIAM Journal on Control and Optimization*, 39(4):1160–1181, 2000.
[20] Ali Awada, Rafic Younes, and Adrian Ilinca. Optimized active control of a smart cantilever beam using genetic algorithm. *Designs*, 6(2):36, 2022.
[21] S. T. Pang, Tsu-Chin Tsao, and Lawrence A. Bergman. Active and passive damping of Euler-Bernoulli beams and their interactions. In *1992 American Control Conference*, pp. 2144–2149. IEEE, 1992.
[22] Jiankang Liu and Bao-Zhu Guo. A novel semi-discrete scheme preserving uniformly exponential stability for an Euler–Bernoulli beam. *Systems & Control Letters*, 134:104518, 2019.
[23] Jim V. Burke, Adrian S. Lewis, and Michael L. Overton. A robust gradient sampling algorithm for nonsmooth, nonconvex optimization. *SIAM J. Optimization*, 15:751–779, 2005.
[24] *Control Toolbox R2021b*. The MathWorks, Inc., Natick, MA, 2021.
[25] Pascal Gahinet and Pierre Apkarian. Structured H_∞ synthesis in MATLAB. In *Proc. IFAC World Congress*, pp. 1435–1440, Milan, Italy, 2011.
[26] *Robust Control Toolbox R2021b*. The MathWorks, Inc., Natick, MA, 2021.
[27] Pierre Apkarian, Pascal Gahinet, and C Buhr. Multi-model, multi-objective tuning of fixed-structure controllers. In *European Control Conf.*, pp. 856–861, Strasbourg, June 2014.
[28] Keat-Choon Goh, Michael G. Safonov, and George P. Papavassilopoulos. Global optimization for the biaffine matrix inequality problem. *Journal of Global Optimization*, 7(4):1573–2916, 1995.
[29] Pierre Apkarian, Dominikus Noll, Jean-Baptiste Thevenet, and Hoang Duong Tuan. A spectral quadratic-SDP method with applications to fixed-order H_2 and H_∞ synthesis. *European Journal of Control*, 10(6):527–538, 2004.
[30] Jean-Baptiste Thevenet, Dominikus Noll, and Pierre Apkarian. Non linear spectral SDP method for BMI-constrained problems: Applications to control design. In *Informatics in Control, Automation and Robotics I*, pp. 61–72. Springer, 2006.
[31] J. Andre C. Weideman and Lloyd Trefethen. Parabolic and hyperbolic contours for computing the Bromwich integral. *Mathematics of Computation*, 76(259):1341–1356, 2007.
[32] Alan M Cohen. *Numerical methods for Laplace transform inversion*, volume 5. Springer Science & Business Media, 2007.
[33] Olof J. Staffans. *Well-Posed Linear Systems*. Encyclopedia of Mathematics and its Applications. Cambridge University Press, 2005.
[34] Kirsten A. Morris. Justification of input-output methods for systems with unbounded control and observation. *IEEE Transactions on Automatic Control*, 44(1):81–85, 1999.
[35] Leonard Meirovitch. *Analytical methods in vibrations*. Series in Applied Mechanics. Macmillan, 1967.
[36] *MATLAB Version: 9.12 (R2022a)*. The MathWorks Inc., Natick, Massachusetts, 2022.
[37] Zhi-Zhong Sun. A finite difference scheme for solving the Timoshenko beam equations with boundary feedback. *Journal of Computational and Applied Mathematics*, 200(2):606–627, 2007.
[38] Zhuangyi Liu and Qiong Zhang. Stability and regularity of solution to the Timoshenko beam equation with local Kelvin–Voigt damping. *SIAM Journal on Control and Optimization*, 56(6):3919–3947, 2018.
[39] Ada Cheng and Kirsten Morris. Well-posedness of boundary control systems. *SIAM Journal on Control and Optimization*, 42(4):1244–1265, 2003.
[40] Kangsheng Liu and Zhuangyi Liu. Exponential decay of energy of the Euler–Bernoulli beam with locally distributed Kelvin–Voigt damping. *SIAM Journal on Control and Optimization*, 36(3):1086–1098, 1998.
[41] Hong Liang Zhao, Kang Sheng Liu, and Chun Guo Zhang. Stability for the Timoshenko beam system with local Kelvin–Voigt damping. *Acta Mathematica Sinica*, 21(3):655–666, 2005.
[42] Metin Gürgöze and Haluk Erol. Dynamic response of a viscously damped cantilever beam with a viscous end condition. *Journal of Sound and Vibration*, 298(1-2):132–153, 2006.
[43] Pierre Le Gall, Christophe Prieur, and Lionel Rosier. Output feedback stabilization of a clamped-free beam. *International Journal of Control*, 80(8):1201–1216, 2007.
[44] Bao-Zhu Guo. Riesz basis approach to the stabilization of a flexible beam with a tip mass. *SIAM Journal on Control and Optimization*, 39(6):1736–1747, 2001.

[45] Thavamani Govindaraj, Jukka-Pekka Humaloja, and Lassi Paunonen. A finite-dimensional controller for robust output tracking of an Euler–Bernoulli beam. In *2022 American Control Conference (ACC)*, pp. 988–993. IEEE, 2022.

[46] Junmin Wang, Bao-Zhu Guo, and Kunyi Yang. Stability analysis for an Euler-Bernoulli beam under local internal control and boundary observation. *Journal of Control Theory and Applications*, 6(4):341–350, 2008.

[47] Huibert Kwakernaak. Mixed sensitivity design. In *45th IEEE Conference on Decision and Control*, pp. 5144–5149. IEEE, 2006.

[48] Sigurd Skogestad and Ian Postlethwaite. *Multivariable feedback design - analysis and design*. Wiley, 1996.

[49] Geir E. Dullerud and Fernando Paganini. *A Course in Robust Control Theory: A Convex Approach*. Springer-Verlag New York, 2000. Springer Texts in Applied Math.

[50] Kemin Zhou, John C. Doyle, and Keith Glover. *Robust and Optimal Control*. Prentice Hall, 1996.

[51] Dominikus Noll. Cutting plane oracles for non-smooth trust-regions. *Pure and Applied Functional Analysis*, 5(3):2020, 671-704.

[52] Pierre Apkarian, Dominikus Noll, and Laleh Ravanbod. Nonsmooth bundle trust-region algorithm with applications to robust stability. *Set-Valued and Variational Analysis*, 24(1):115–148, 2016.

[53] Pierre Apkarian and Dominikus Noll. Nonsmooth optimization for multiband frequency domain control design. *Automatica*, 43(4):724 – 731, 2007.

[54] Martin Hast, Karl Johan Åström, Bo Bernhardsson, and Stephen Boyd. PID design by convex-concave optimization. In *2013 European Control Conference (ECC)*, pp. 4460–4465. IEEE, 2013.

[55] Alireza Karimi and Christoph Kam. A data-driven approach to robust control of multivariable systems by convex optimization. *Automatica*, 85:227–233, 2017.

[56] Pauline Kergus, Charles Poussot-Vassal, Fabrice Demourant, and S Formentin. Frequency-domain data-driven control design in the Loewner framework. *IFAC-PapersOnLine*, 50(1):2095–2100, 2017.

[57] Duncan C. McFarlane and Keith Glover. *Robust controller design using normalized coprime factor plant descriptions*, vol. 138. Springer, 1990.

[58] Duncan C. McFarlane and Keith Glover. A loop shaping design procedure using H_∞ synthesis. *IEEE Trans. Aut. Control*, 37(6):759–769, 1992.

[59] Pierre Apkarian and Dominikus Noll. Nonsmooth optimization for multidisk H_∞ synthesis. *European Journal of Control*, 12(3):229–244, 2006.

[60] Pierre Apkarian and Dominikus Noll. Nonsmooth H_∞ synthesis. *IEEE Trans. Aut. Control*, 51(1):71–86, 2006.

[61] Dominikus Noll. Bundle method for non-convex minimization with inexact subgradients and function values. *Springer Proceedings in Mathematics & Statistics*, 50:555–592, 2013.

[62] Benedict Dingfelder and JAC Weideman. An improved Talbot method for numerical Laplace transform inversion. *Numerical Algorithms*, 68(1):167–183, 2015.